Ultra-sensitive NO2 gas sensors based on single-wall carbon nanotube field effect transistors: Monitoring from ppm to ppb level

Leandro Sacco, Salomé Forel, Ileana Florea, Costel-Sorin Cojocaru

L. Sacco, Salomé. Forel, I. Florea, C.-S. Cojocaru, Ultra-sensitive NO_2 gas sensors based on single-wall carbon nanotube field effect transistors: Monitoring from ppm to ppb level, *Carbon* (2019), doi: https://doi.org/10.1016/j.carbon.2019.10.073.

Ultra-sensitive NO_2 gas sensors based on single-wall carbon nanotube field effect transistors: Monitoring from ppm to ppb level.

Leandro Sacco [a,1,], Salomé Forel[a,2], Ileana Florea[a], Costel-Sorin Cojocaru[a]*

a Laboratoire de Physique des Interfaces et des Couches Minces (LPICM), CNRS, Ecole Polytechnique, IP Paris, 91128, Palaiseau Cedex, France

***Corresponding Author at** : Delft University of Technology, Faculty of Electrical Engineering, Mathematics and Computer Science, Department of Microelectronics, Delft, Feldmannweg 17, 2628 CT Delft, Netherlands mail : l.n.sacco@tudelft.nl

Present Addresses

1 Delft University of Technology, Faculty of Electrical Engineering, Mathematics and Computer Science, Department of Microelectronics, Delft, Feldmannweg 17, 2628 CT Delft, Netherlands

2 Antwerp University, physics departement, Experimental Condensed Matter Physics Laboratory, Universiteitsplein 1, 2610 Antwerp Belgium

L. Sacco, Salomé. Forel, I. Florea, C.-S. Cojocaru, Ultra-sensitive NO_2 gas sensors based on single-wall carbon nanotube field effect transistors: Monitoring from ppm to ppb level, *Carbon* (2019), doi: https://doi.org/10.1016/j.carbon.2019.10.073.

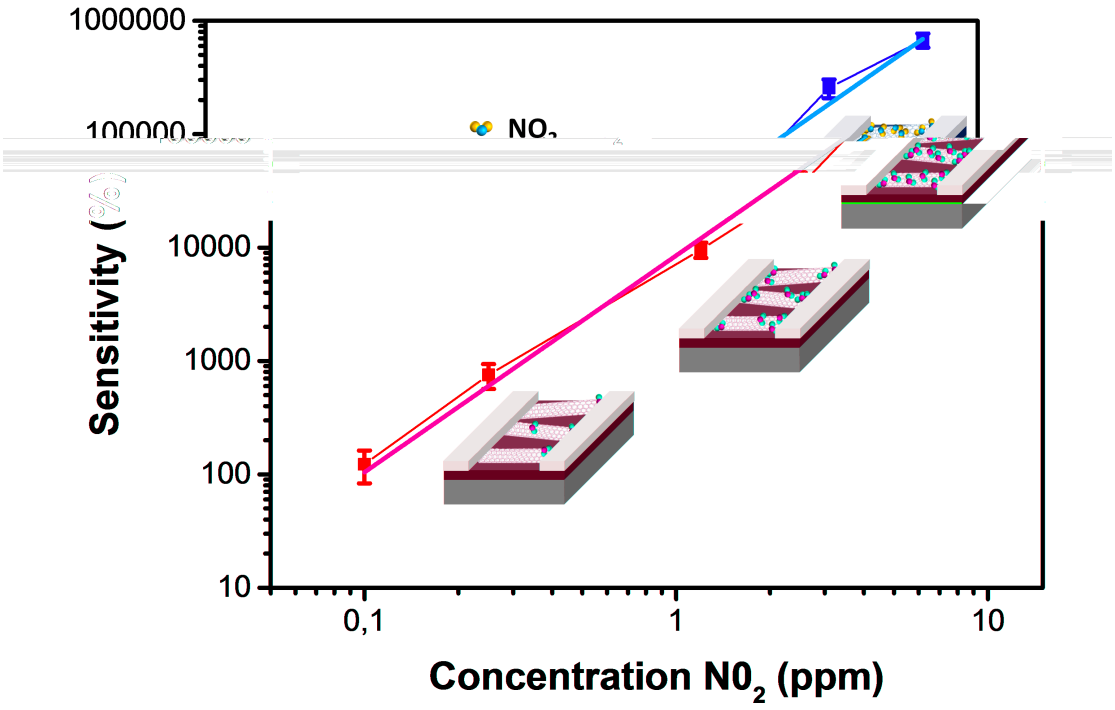

Owing to their sensitive chemical-to-electrical transducer capabilities and compatibility with deviee miniaturization and low operation temperature, single-walled carbon nanotube field-effect transistor (SWCNT-FET) represents an attractive platform to provide solutions in the gas sensing field. In this work, SWCNT-FETs were fabricated and their performances for detecting low NO_2 concentrations were evaluated. Outstanding deviees response was obtained, which was shown to follow a 2 power law dependence between the response and the NOz concentration in the range of 100 ppb up to 10 ppm. Such ultra-high response is attributed to an enhancement of the Schottky barrier modulation triggered by the specifie deviee configuration. The deviee configuration is based on individual semiconducting SWCNTs directly connecting the interdigitated Source-Drain electrodes. To the best of our knowledge, the results reported here correspond to the most sensitive deviee among the deviees based on non-functionalized carbon materials and operational at low temperatures. Furthermore, the obtained results are supported by a deep SWCNT characterization, and the changes in Schottky barrier's height induced by the,presence of gas molecules are estimated and discussed. Overall, the present reported results provide useful information for establishing a robust process for the fabrication of the next generation of CNT based gas-sensing devices.

1. Introduction

Nitrogen dioxide (NO_2) molecules in gas phase have significant negative impacts on human health and for the environment, as the major sources of nitrogen dioxide are the result from anthropogenic activities, the detection of NO_2 gas has emerged over the past decades as one of the most critical sensing applications. Generally speaking, technological evolution in the field of gas sensing requires reasonable manufacturing prices, fast responses, and portable devices. To this respect, the bulky size and high cost of conventional gas detectors, such as gas chromatography-mass spectrometry (GC-MS) and Fourier transform infrared (FT-IR) spectrometry severely limit their use for portable applications. On the other hand, gas sensor technologies based on metal-oxides (MO_X) are characterized by small size devices, high responses, and low implementation costs for detecting concentrations in the parts-per-million (ppm) range. Nevertheless, sensors based on MO_X-technology, tipically operate at temperatures higher than 200°C, with a corresponding increase in power consumption [1] during operation and related increase of packaging/deploying difficulties. Gas sensors based on nanomaterials arise as an attractive solution to reliably detect, recognize and differentiate various gas concentrations [2–5] and they constitute a new class of low power consumption and miniaturized devices. Particularly, single wall carbon nanotube field-effect transistors (SWCNT-FET), are a very attractive gas sensing platform [6,7], since the interaction between the analyzed gas and carbon nanotubes affects their electrical conductance even at very low analyte concentrations, thus enabling direct conversion to an electrical signal. Many studies have been devoted to empirically determine the response of SWCNT-FETs towards various gases and under various operation conditions [8–10]. Although most efforts have been focused on elucidating the electrical response of SWCNT-FETs, their exact gas sensing mechanism is still an open question. During the past years, as an attempt to isolate and identify the active element of the sensing mechanism, remarkable contributions have been obtained by selective passivation of different parts of the transistor, to block their gas exposure, for example to NO_2 [11,12] and ammonia (NH_3) [13]. The overview of these experiments consolidate the idea that the sensing phenomena takes place mainly through the adsorption of gas molecules at the metal/SWCNT interface, rather than on the body of the nanotube. Therefore, the measured changes of the current through the device are to be attributed to the adsorbed gas molecules at the metal/SWCNT electrode interface that modify the Schottky barriers of the nanotube and the metal

electrodes [14]. Such results concern SWCNT-FET-based sensors fabricated using individual SWCNT, however, this fabrication approach, from a technological point of view, leads to several limitations [6]. Therefore, the main body of the reported studies have been focused on the use of percolated SWCNT networks between the source and drain electrodes. The semiconducting behavior of the channel is then obtained either by controlling the areal density of the network and the mean SWCNT length [15] or by applying a selective electrical breakdown to remove the metallic tubes from the network [16]. Once again using the passivation technique, it has been proven that in this case, the changes in the device conductance are highly affected by the SWCNT–SWCNT junctions[12].

In the present work, we introduce an approach for gas sensing device conception that combines the benefits of individual SWCNT-FET and the increased sensitive area and channel current of SWCNT network based devices. In our approach, several individual SWCNTs are directly connected between the source and drain electrodes leading to a high increase of the device response as compared to previously reported sensors based on single tubes [17,18] or dense networks [10,19,20]. Table 1 summarizes representative works of NO_2 gas sensors based on SWCNT-FET operational at room temperature and without functionalization. Table 1 accounts for the device architecture, the adopted response definition, and the device response at their minimum NO_2 concentration. Basically, two different approaches have been adopted regarding the device architecture: sensors based on individual SWCNT [21–23] and sensors based on networks of SWCNTs [10,24,25]. However, the device configuration based on several isolated SWCNTs connected between the source/drain electrodes does not seems to have been explored for gas sensing measurements, notwithstanding that some devices adopting this configuration have been fabricated for other applications [26–29]. In this work, the obtained results show that such implemented device configuration significantly increases the number of active sites at the metal/SWCNT junctions leading to a huge response of the device when exposed to NO_2 molecules. As a result, the gas-sensing devices presented in this work are amongst the most sensitive reported gas sensors based on carbon nanostructures, operating at room temperature and without functionalization[9]. The approach we propose aims to set the basis for the fabrication of next generation gas sensors based on carbon nanostructures, while simultaneously allowing access to simple tools to calculate the influence of the gas concentration on the Schottky barrier height.

Device Architecture	Response definition	Limit of Detection (LOD) [ppm]	Minimum measured Concentration [ppm]	Response at minimum concentration	Sensitivity [1/ppm]	Response (R) Vs Concentration (C) $log(R) = \log(a) + b\log(C)$	Art.
FET sensors based on individual SWCNT	R_{N_2}/R_{NO_2}	-	200	10	-	-	[21]
FET sensors based on individual SWCNT	$\frac{R_{NO_2} - R_{N_2}}{R_{N_2}}$	-	0.3	2	-	-	[22]
FET sensors based on Individual, suspended SWCNT	$\frac{I_{NO_2} - I_{N_2}}{I_{N_2}} x100\%$	-	1	115 %	-	-	[23]
FET sensors based on SWCNT networks	$\frac{I_{NO_2} - I_{N_2}}{I_{N_2}} x100\%$	-	20	10 %	-	-	[10]
FET sensors based on SWCNT networks	$\frac{G_{NO_2} - G_{N_2}}{G_{N_2}}$	0.044	6	6	0.034 ± 0.002	-	[24]
FET sensors based on SWCNT low density networks	I_{NO_2}/I_{N_2}	-	0.86	3	-	-	[25]
FET sensors based on few SWCNTs individually connected	$\frac{I_{NO_2} - I_{N_2}}{I_{N_2}} x100\%$	0.086	0.1	100%	-	log(a)= 3.92 ± 0.05 b= 1.90 ± 0.10	Present work

Table 1. Response definition, minimum measured concentration value and sensitivity value of NO_2 gas sensors based on SWCNT-FET operated at room temperature with different device architectures.

2. Material and methods

2.1 SWCNT synthesis

SWCNT synthesis was carried out by double-hot-filament-assisted chemical vapor deposition (dHF-CVD) technique[30] in a horizontal tube furnace following similar procedure described in our previous works[31,32]. Briefly, 200 nm thermal silica coated silicon wafers (SiMat) used as

support for the SWCNT CVD growth were cleaned, functionalized and covered with a monolayer of Nickel-Ruthenium (NiRu) Prussian blue analog (PBA) used as a pre-catalyst [31,32]. For each experiment, before introducing the methane (CH_4) carbon source, the system was pre-heated from room temperature to 900°C. Once reaching this temperature, activated hydrogen (H_2) was introduced into the reactor and a pretreatment step under 100 sccm H_2 at 90 mbar was performed for 5 minutes in order to reduce the PBA nanoparticles into bimetallic nanoparticles which are the effective catalyst. Finally, CH_4 was added into the reactor as carbon source for approximately 30 min at 100 mbar pressure with a flow rate of 20 sccm and the activated hydrogen flow rate was set at 100 sccm, both hot-filaments being activated with power supplies of 120 W and 160 W, respectively for CH_4 and H_2.

2.2 SWCNT characterization

A HORIBA LabRam ARAMIS Raman spectrometer, using a ×100 objective, with four excitation wavelengths (473 nm, 532 nm, 633 nm, and 785 nm) was used to evaluate the crystalline quality of the synthesized SWCNT and their diameter distribution (see **Figure 1** and **Figure S1**). For each laser line, 484 spectra have been recorded. The SWCNT diameter distribution has been extracted using the empirical law reported by Jorio [33] and co-workers, expressed as $\omega RBM = 248/dt$, where ωRBM is the resonance frequency of the nanotube on the radial breathing mode (RBM) expressed in cm^{-1} and dt is the tube diameter expressed in nanometer. The reproducibility of the obtained diameter distributions have been reported in previous work[32].

High resolution TEM (HRTEM) analyses were performed in order to examine the morphology of SWCNTs (see **Figure S2**). The observations were performed on a 300 kV environmental transmission electron microscope (E-TEM) TITAN equipped with a spherical aberration corrector (Cs) on the image. All the observations were performed at 80kV in order to reduce the beam effects.

The SWCNT density was examined by scanning electron microscopy (SEM) on a HITACHI S 4800 electron microscope operating at 1 kV and 10 mA.

2.3 Device fabrication

The main benefit of achieving CVD growth on Si/SiO_2 wafer substrates is that it easily allows direct integration of the synthesized SWCNTs in a bottom gate FET device configuration without use of additional transfer technique. In our devices (see **Figure 2a and Figure S3** in SI for schematic view of the device), the doped silicon was used as a back gate and the interdigitated (1 mm equivalent length) palladium (Pd) contacts, acting as source and drain, were directly evaporated on thermal silicon oxide layer using simple UV lithography technique. Briefly, after three minutes of sonication in acetone and isopropanol, a photosensible resin (SU_8) was spin-coated for about 30 seconds at 4000 rpm. The wafer was then annealed for 5 min at 110°C under air. A patterned quartz mask was used to perform selective UV illumination. The mask/sample system was afterwards illuminated under UV for 7 seconds at 10 mW. The sample was then immersed for 25 seconds in a solution of MF-319, where the UV-exposed resin was removed. Finally, 40 nm of palladium were evaporated over the sample, and boiling acetone was used to remove the non-irradiated resin. At the end of the process, the devices were cleaned using a boiling isopropanol solution.

In order to eliminate all the metallic SWCNTs from the conduction channel, a preliminary step based on selective electrical breakdown technique was applied[16]. This technique consists of applying a high voltage between the source and drain after protecting the semiconducting SWCNTs by applying an adapted gate voltage. Here, we fixed the gate voltage at 15 V and the voltage between the source and drain gradually swept between 0 and 20V. A statistical analysis of the characteristic of our devices has been reported in prior work[32].

2.4 Electrical Measurement

The electrical measurements were performed using a semiconductor parametric Keithley 4200-SCS analyzer. For all the recorded I_{ds}-V_g transfer curves, a fixed bias voltage of 1V was applied between the source and drain (V_{ds}). A voltage sweep was applied from -20V to +20V with a step of 0.05V to the gate electrode (V_g), and the current flowing between source and drain (I_{ds}) was monitored. Our devices present a hysteresis (see **Figure S4** in supporting information), all the measurements have been carried on a complete cycle, however, the effect of the hysteresis has not been accounted for analysis and only forward sweeps (from -20 to +20V) have been considered for the following data analysis.

2.5 Gas exposure

Gas exposure experiments were performed using an Owlstone gas generator (OVG-4) based on permeation tube technology. Fine-tuning of the tube permeation rate, the temperature and the selected flow rate, enable very precise control of the concentration level. For our study, two NO_2 permeation rates of 2425 ng/min and 102 ng/min were used, at temperatures set between 30°C and 40°C. For all our experiments the NO_2 gas was diluted in dry N_2 to reach the desired concentrations. The gas generator is connected to a homemade hermetic chamber of approximatively 65l volume (see **Figure S5** in SI). The temperature of the device was fixed at 20°C using a Huber mini-stat 125 and 1bar pressure was imposed during measurements. The analyzed gas was flown through a 4 mm diameter circular holed pipe (see SI for technical information concerning the gas delivery system). During exposure, in real time, I_{ds}-V_g transfer curves of the SWCNT-FET were measured using a semiconductor parametric analyzer Keithley 4200-SCS. After a defined exposure time of the device to the NO_2/N2 mixture, the device is exposed to a constant flow of pure N_2 (2L/min) inducing the desorption of the NO_2 molecules attached to the device. The gas desorption is also analyzed through the measurement of the I_{ds}-V_g characteristic (see figure S6 in SI).

The reproducibility of the sensors was tested using other device fabricated following the same processing steps but from a different fabrication batch. The response as a function of the concentration in the range of 0.05-10 ppm was calculated, allowing to compare the calibration curve of both devices (see figure S7 in SI). The stability of the gas sensor was evaluated by comparing measurements at 4 months difference, of the transfer curves of the same device, under pure N_2 atmosphere and respectively exposed to 0.25 ppm NO_2. For both sets of measurements the device response was the same (see figure S8 in SI).

2.6 Calculation of the Device Response

The sensing performance of SWCNT-FET was evaluated according to the response (R) as expressed in equation 1, defined by the relative to the drain current change, as the percent change in current divided by the initial current in different gas concentrations:

$$R = \frac{I_{OFF}(NO_2) - I_{OFF}(N_2)}{I_{OFF}(N_2)} * 100\% \quad (1)$$

Here I_{OFF} (N_2) represents the average value of the current obtained for a gate voltage (V_g) sweep between +19 V and +20 V under constant N_2 flow, and I_{OFF} (NO_2) represents the average value of the current obtained for the same V_g sweep range after exposure to a defined concentration of NO_2.

As defined, the device response is proportional to the surface coverage of adsorbed NO_2 molecules, that can be expressed as a Freundlich isotherm adsorption, which is an empirical model for multisite adsorption on rough surfaces. The device response (R) can then be parametrized in terms of the NO_2 concentration (C_{NO_2}) as given in equation (2):

$$R = a\ C_{NO_2}^{b} \quad (2)$$

Where a and b are constants.

2.7 Schottky barrier height calculation

Mainly two components contribute to the charge transport through a SWCNT-FET with a Schottky barrier: the thermionic emission current (over the Schottky barrier) and the tunneling current (through the depletion region) [34]. The band bending diagram at the metal–SWCNT interface is illustrated in Fig.S9 (see SI) with their respective I_{ds}-V_g transfer curve. To calculate the effective barrier height, we consider the thermionic emission over the Schottky barrier to be the dominant transport mechanisms, which is expected to be the case when the gate voltage is in the subthreshold regime. Under this conditions, the drain-source current satisfies Eq.(3):

$$I_{ds} \sim T^2 e^{q(\phi_B - \Delta\phi)/KT} \quad (3)$$

Where ϕ_B is the Schottky barrier height, K is the Boltzmann constant, T is the absolute temperature, and $\Delta\phi$ the image force barrier lowering.

Then, for the gate voltage in the subthreshold regime, the channel current can be simplified as expressed in Eq.(5) [35],

$$I_{ds} = AA^* T e^{q(\phi_B)/KT} \quad (4)$$

Where AA* is the product of the contact area (A) and the effective Richardson constant (A*). The activation energy method is the most used procedure to measure Schottky barrier heights

in SWCNT-metal contacts[36,37]. The main advantage of this procedure relies on the fact that it does not require an estimation of the electrically active junction between the metal electrodes and the carbon nanotubes. However, the extracted height barrier depends on the identification of the flat-band voltage (V_{FB}). At this potential, no band bending occurs at the metal/SWCNT junction at the source electrode, but its exact determination is quite challenging, especially for materials with a low effective mass, such as SWCNTs [38]. Consequently, the activation energy method provides a simple procedure based on drain current measurements at different temperatures, to roughly extract the Schottky barrier height. However, more sophisticated procedures need to be applied[39,40] for more precise calculations.

In order to bind together the Schottky barrier with the gas sensor response, it is of paramount importance to point out that the device response in the band bending regime has to be avoided, therefore, the device response has to be evaluated around the flat-band Voltage. Accounting the response from Eq.(1) when evaluated around the flat-band Voltage ($R_{V_{FB}}$) instead of the depletion regime, equation (1) and (2), turns as express equations (5) and (6):

$$R_{V_{FB}} = \frac{I_{V_{FB}}(NO_2) - I_{V_{FB}}(N_2)}{I_{V_{FB}}(N_2)} * 100\% \quad (5)$$

$$R_{V_{FB}} = a_{V_{FB}} C_{NO_2}^{b_{V_{FB}}} \quad (6)$$

Where $I_{V_{FB}}(N_2)$ and $I_{V_{FB}}(NO_2)$ represents the average value of the measured currents under a pure nitrogen atmosphere and respectively after 15 min of exposure to a defined concentration of NO_2, both obtained at gate voltage set to V_{FB}. The $a_{V_{FB}}$ and $b_{V_{FB}}$ are constants obtained from the power law fit of the device response, at V_{FB}, function of the NO_2 concentration.

By combining Eq.(4) with the equations of response (5) and (6), it is possible to obtain a relation evidencing the dependence of the Schottky barrier height when exposed to NO_2 gas molecules (ϕ_{B-NO_2}) as a function of the Schottky barrier height when under a N_2 atmosphere (ϕ_{B-N_2}) and the NO_2 concentration, as expressed in Eq.(6) bellow:

$$\phi_{B-NO_2} = \phi_{B-N_2} - KTln[\frac{1}{100} a_{V_{FB}} (C_{NO_2})^{b_{V_{FB}}} + 1] \quad (6)$$

The extracted Schottky barrier value ϕ_{B-N_2} can be further calculated by measuring device transfer curves at various temperatures. These set measurements enable one to obtain Arrhenius–type plots ($\ln\left(\frac{I_{ds}}{T}\right) vs \left(\frac{1}{KT}\right)$) for different gate voltages.

3. Results and Discussion

3.1 SWCNT characterization

SWCNTs have been synthesized using a double-hot-filament-assisted chemical vapor deposition (dHF-CVD) process (see experimental section). Prior to their integration in devices, using Raman spectroscopy with four excitation wavelengths (see **Figure 1.a-c** and **Figure S1** in SI), the diameters of SWCNTs were estimated between 0.8 and 2.2 nm (see **Figure 1.d**). The analysis of the D and G bands clearly indicates the good crystallinity of the obtained SWCNTs as the intensity I_D/I_G ratio is always lower than 15% (see **Figure 1.c**).

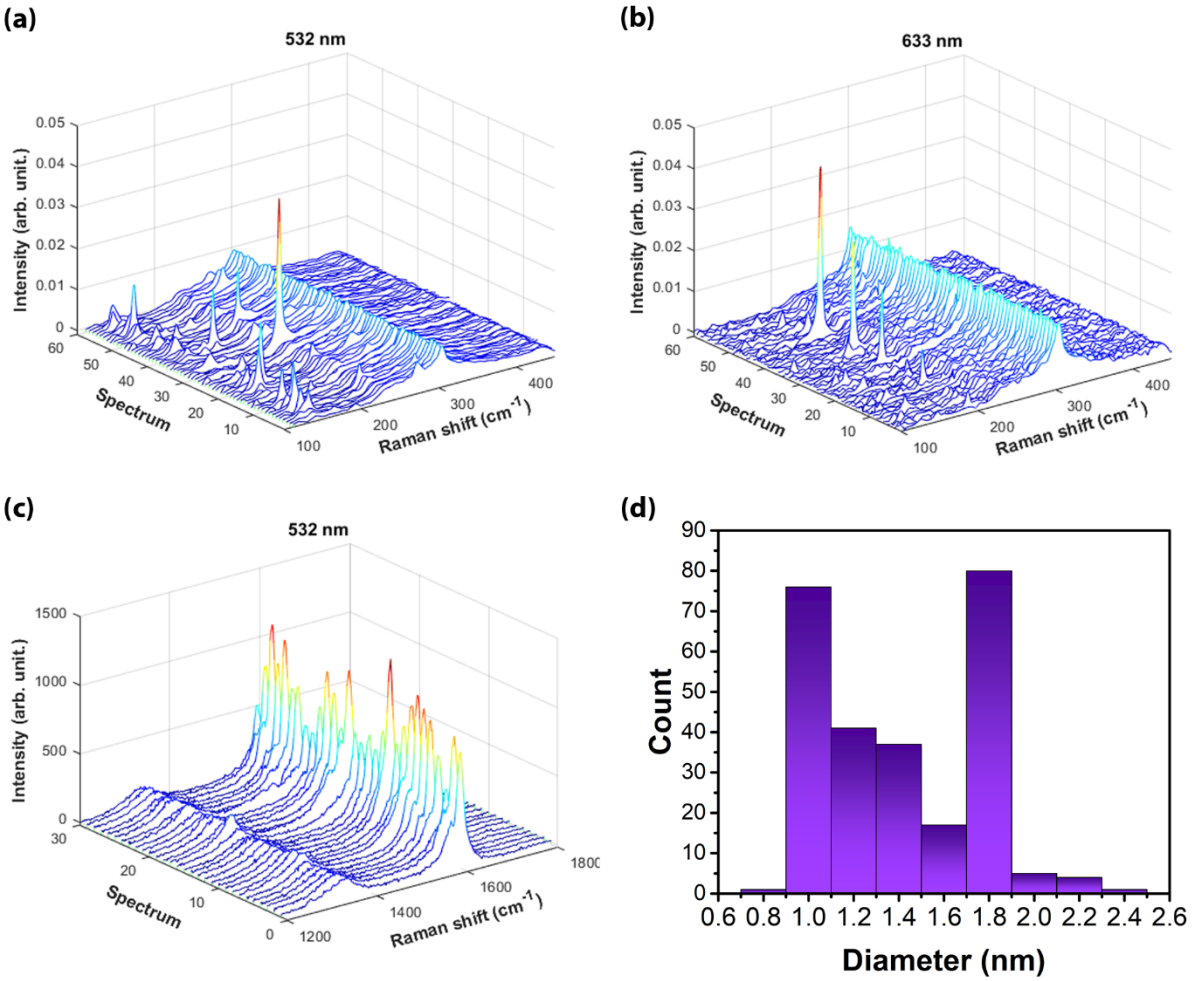

Figure 1. Characteristic Raman spectrum of SWCNTs in the RBM range for an excitation at (a) 532 nm (b) 632 nm (c) characteristic Raman spectrum of SWCNTs in the DG range for an excitation at 532 nm (d) SWCNT diameter distribution extracted from the RBM peaks obtained with excitation at 473 532nm, 632 nm and 785 nm.

The low defect density in SWCNTs was further confirmed through transmission electron microscopy (TEM) analysis, a typical image of SWCNT obtained by the same synthesis process is available in **Figure S2.**

3.2 Gas sensing measurements

The source and drain electrodes were deposited directly on the as-synthesized SWCNTs (see experimental section for details). An electrical breakdown process (see experimental section) was performed in order to disconnect potential metallic SWCNTs connected between the electrodes.

The presence of several SWCNTs directly connected between source and drain was confirmed by SEM images (see **Figure 2.b**).

The conductance response of the fabricated devices, as exposed to various NO_2 concentrations, was then examined. For consistency reasons, in the following section, only results obtained on one of the devices will be presented, but similar results have been obtained as shown in the SI (see Figure S7), for other device from a different fabrication batch fabricated following the identical processing steps.

Using a dedicated ultra-high vacuum (UHV) type testing chamber (see section Material and methods 2.5), the reference signal response of the device was measured under dry N_2 atmosphere and one can notice that the SWCNT-FET presents a typical p-type behavior, with an I_{on}/I_{off} ratio of 10^5 (see black curve transfer in **Figure 2.c**). The transfer curves obtained by exposing the devices to different NO_2 concentrations are presented in **Figure 2.c** where an increase of the current in the depletion mode as the NO_2 concentration increase is clearly evidenced. From the transfer curves it can be easily inferred that the device reacts to concentrations as low as 0.05 ppm since the threshold voltage is shifted (see the red curve on **Figure 2.c**).

Nevertheless, a threshold voltage variation can be eventually generated from fixed charges present on the gate oxide surface close to SWCNT, [41] and then this may induce errors or uncertainties if used as only criterion for the response of the sensor. Consequently, threshold voltage variation has been not used to characterize the sensor response and we choose to use the modification of the current in the off-state as criterion to define the device response upon gas exposure (see Eq.(1)). The device response as a function of the NO_2 gas concentration is represented in **Figure 2.d**. Using the dependence of the intensity of the Off-current (within the gate bias range of 19-20V) as a criterion, allows us to infer that the device is able to detect a NO_2 gas concentration nearby 0.1 ppm with an 100% increase of the drain current for the gate voltage sweeping range (19-20V) To our knowledge such extremely high response has never been reported in previous works based on carbon nanostructures [9] and particularly for studies of NO_2 gas sensors based on SWCNT-FET (see table 1).

Previous reported studies suggested that the sensing mechanism takes place at the metal electrode/SWCNT interface[11,13,18,42]. The explanation for this phenomenon relies on the fact

that the adsorbed gas molecules induce changes on the Schottky barriers formed at the junction of the nanotube and the electrodes. The adsorption of NO_2 molecules is expected to increase the work function of the Pd electrodes thus leading to reduction of the barrier height associated to hole carriers, consistent with an increase of the I_{OFF} as the NO_2 concentration increases. A tailed model of the hole carrier using Pd electrodes is provided by Perello et al.[43]. They propose a surface inversion channel (SIC) model that considers a carrier transport within the contact-covered section of the SWCNT. The SIC model eliminates inconsistencies related to the conduction in extremely low work function metals.

In our system, the response calculated in the depletion zone depicts an exponential trend as a function of the NO_2 concentration (C_{NO_2}) (see **Figure 2.d**), which can be parametrized by equation (2).

A linear regression extracted from the log-log plot (**Figure 2.d**) indicates approximately a 2 power law relation between the response and the NO_2 concentration, evidencing the huge response of the device. In this depletion regime the source-drain current is purely thermionic [34], and can be expressed as shows in the equation (3).

Assuming that $\Delta\phi$ mainly depends on the applied potential, the response (Eq.(1)) can be expressed as a function of the Schottky barrier's height. By replacing Eq.(3) in the response defined by Eq.(1), the response is then expressed in terms of the Schottky barrier's heights under different gas atmospheres (see equation (7)):

$$R \sim e^{q(\phi_{B-N_2}-\phi_{B-NO_2})/KT} - 1 \quad (7)$$

The exponential dependence of the response as a function of NO_2 concentration can then be attributed to a Schottky barrier modulation. In our device, the response is also enhanced by the specific design of the device. Usually, gas sensors based on SWCNT-FET either consist of one single tube connected between the source and drain electrodes, or a dense (random) network of SWCNT. However, such device configurations present different limitations. In the case of single tube devices, the active sites for NO_2 are limited by the metal/tube[44,45] interface. On the other hand, for devices based on percolated tubes, the response is affected by metallic tubes and/or SWCNT junctions that hinder or suppress the effect of metal/SWCNT Schottky barrier modulation[10,12]. The device design in this work avoids these problems induced by percolation

and simultaneously increases significantly the available active sites surface since several tubes are individually connected between the electrodes as illustrates **Figure 2.b**.

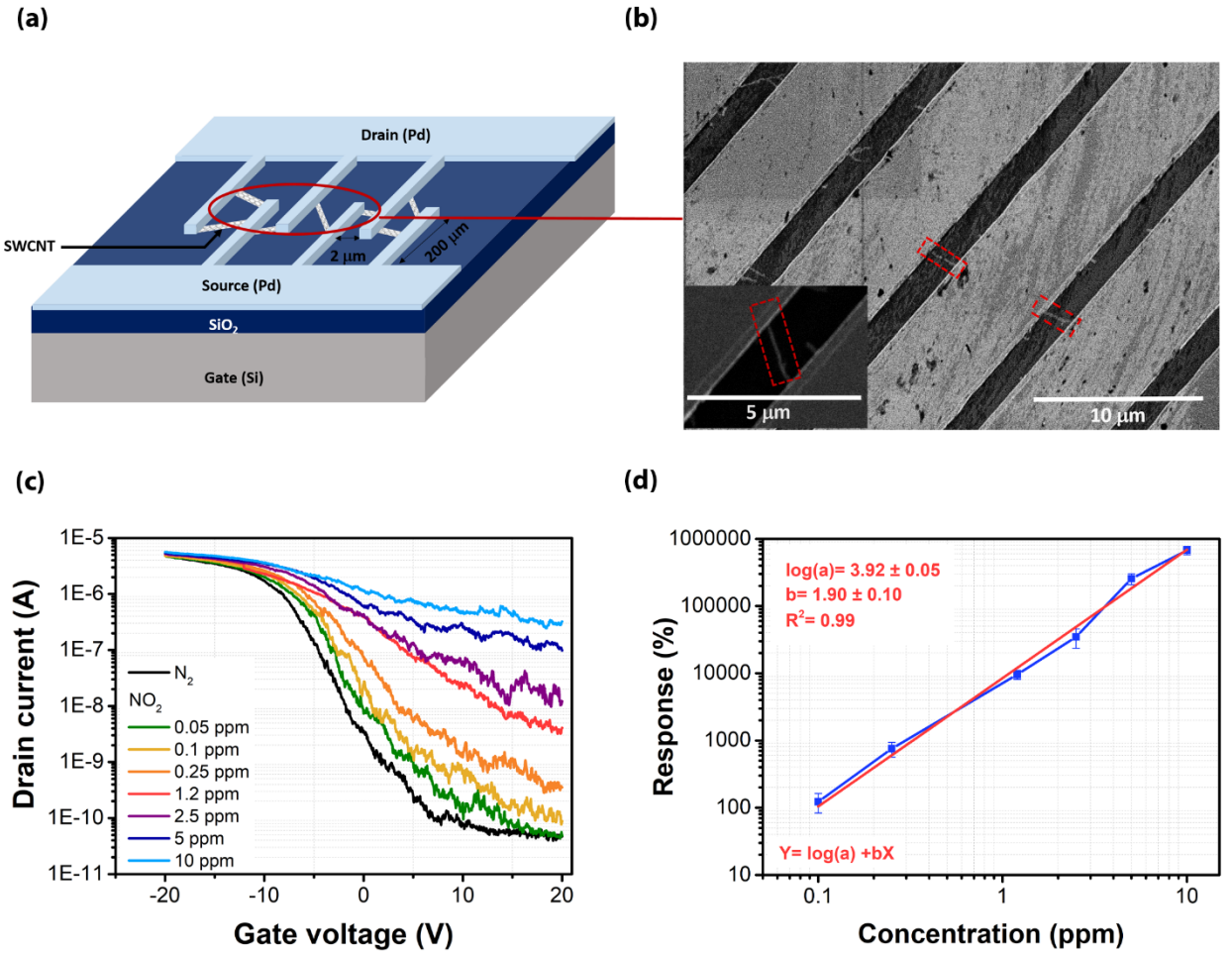

Figure 2. (a) Scheme showing the architecture of the device (b) SEM micrograph showing individual SWCNTs connecting the source and drain electrodes (Inset individual SWCNT connecting Pd electrodes). (c) Transfer characteristics under various NO_2 concentrations of our SWCNT- FET, with tubes connected individually between the source and drain electrodes. All curves were measured after 15 minutes of gas flow stabilization. (d) Response as a function of NO_2 concentration.

An important figure of merit in chemical sensing is the limit of detection (LOD). LOD is expressed as a concentration corresponding to the smallest signal that can be detected with a reasonable certainty, such value is given within a stated confidence level confidence factor (η) times the standard deviation (σ) of the background signal. The detailed explanation for the

calculation of the LOD is shown in the SI. From the linear fit of **Figure S10**, with confidence value $\eta = 1.645$, which corresponds to a 90% confidence level, the LOD was finally estimated to be 0.086 ppm. This result is consistent with the measurements shown in **Figure 2.c** because as we previously mentioned, the device is sensitive under exposure of NO_2 0.05 ppm (for instance the threshold voltage is shifted) but not for the adopted criterion to quantify the device response (there is no change in the drain current within the range of gate voltage 19-20V).

3.3 Schottky barrier modulation

A deep understanding of the properties of metal/semiconductor junctions still remains a current challenge for further implementation of Schottky diodes in nano-electronics since such interface effects dictate device behavior. Basic considerations of semiconductor gas sensors still remain controversial when applied to nanodevices because most of the theoretical results based on Schottky barriers are difficult to compare with experimental data due to simplified geometry that underestimates the nature of junction[46]. Herein, we introduce a basic calculation in order to obtain an estimate of the influence of the gas molecules concentration upon the Schottky barrier height, as explained in section 2.7.

The extracted Schottky barrier height for ϕ_{B-N_2} is calculated by measuring device transfer curves at various temperatures (see **Figure 3.a**). From these measurements, Arrhenius–type plots ($(\ln\left(\frac{I_{ds}}{T}\right) vs\ (\frac{1}{KT})$)) are constructed for different gate voltages (see **Figure 3.b**). For a drain-source applied voltage (V_{ds}) of 1V, the slope of the resulting plot $\ln\left(\frac{I_{ds}}{T}\right) vs\ (\frac{1}{KT})$ is equal to the Schottky barrier height. The tunneling current can only be neglected when the gate voltage is below the flat-band voltage. On the contrary, thermally assisted tunneling contributes to the transport due to a large band bending which is not included in the standard thermal emission theory[47]. At the V_{FB} the band diagram is not affected by tunneling currents and only the thermionic contribution is responsible for the transport in the conduction channel. Then, the energy activation at this voltage corresponds to the effective Schottky barrier height. For gate voltages higher than the V_{FB}, the activation energy increases linearly. The V_{FB} corresponds to the gate voltage at which a deviation from the linear trend is observed, as depicted in **Figure 3.c**. Since the devices do not exhibit significant ambipolar characteristics, the activation energy saturates for positive gate voltages, showing that no tunneling contributions are detected as no conduction in the n-branch is observed.

The extrapolated value of the Schottky barrier height under a N_2 atmosphere is ϕ_{BN_2}= 100 meV, which is in good agreement with previous works, where a Schottky barrier height of 150 meV has been obtained for a system with Pd contact and a mean diameter of SWCNTs around 1.4 nm [46,48]. Moreover, this relatively low value is consistent with the high ON and low OFF currents of our device that is also characteristic for transistors with low Schottky barrier heights. On the contrary, higher Schottky barrier values for one type of carriers leads to a decrease of the Schottky barrier height for the opposed type of charges, thus, the Fermi level of the metal is positioned closer to the middle of the band gap resulting in ambipolar characteristics with a significant contribution from both hole and electron currents, which, as mentioned previously, is not observed in the transfer curves presented in **Figure 2.c** and **3.a**.

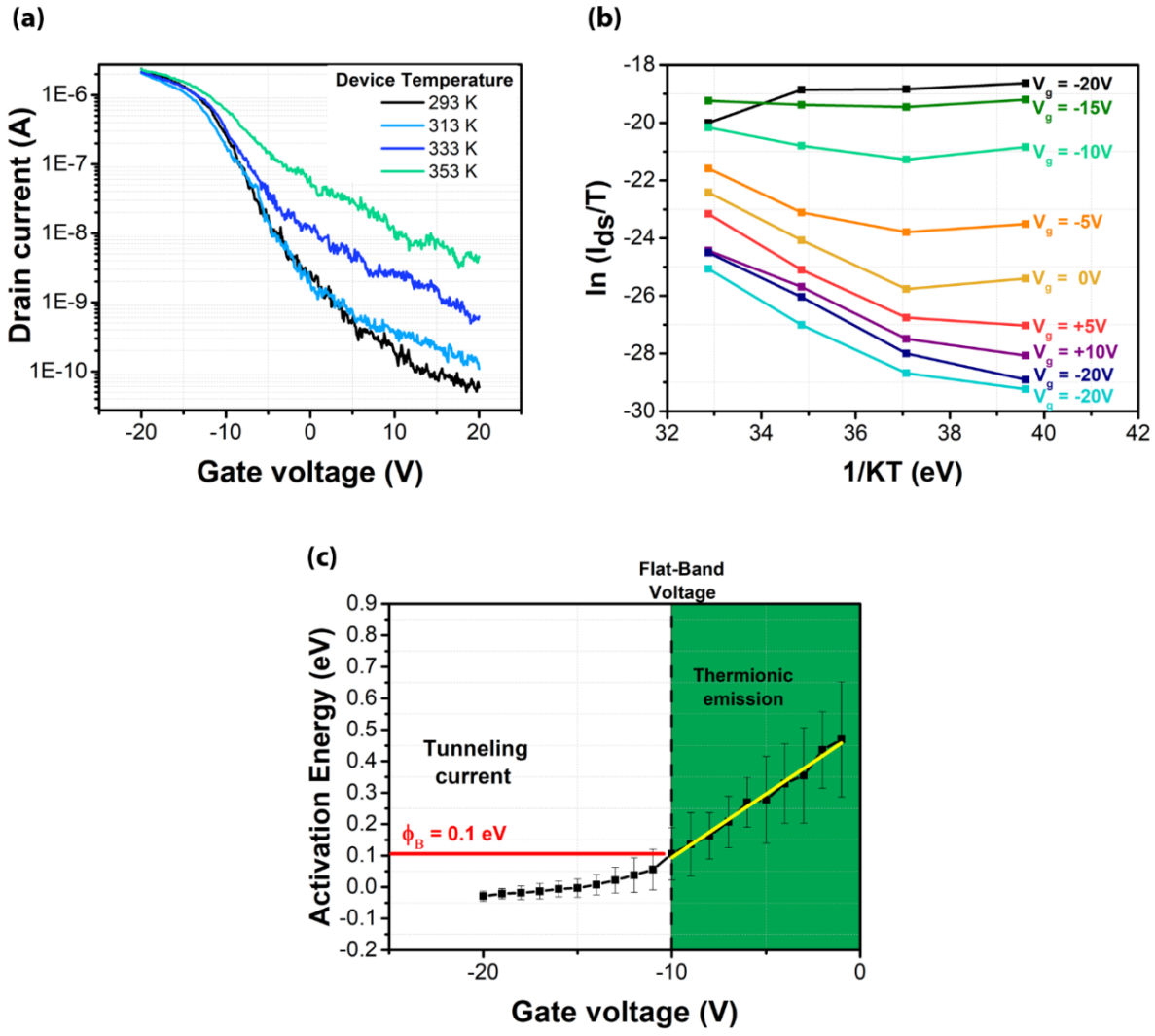

Figure 3. Extraction of the effective Schottky barrier height. (a) Transfer curve at different operational temperatures. (b) Arrhenius plot at various voltage gate. (c) Schottky barrier height as a function of gate voltage (V_g), the effective Schottky barrier height is obtained at the flat-band voltage.

The modulation of the Schottky barrier height expressed in Eq.(6) is valid only for applied potentials close to the flat-band voltage. From this point of view, it is then necessary to calculate the response around the V_{FB}, and fit the curve of the response as a function of NO_2 concentration, in order to extract the $a_{V_{FB}}$ and $b_{V_{FB}}$ constants as shown in **Figure 4.a**. Then, the variation of the Schottky barrier height as a function of the NO_2 concentration could be obtained as depicted in **Figure 4.b**. As expected, a decrease of the barrier height is observed when the NO_2 concentration increases and we assume that this phenomenon can explain the behavior of our device under the NO_2 exposure and its observed high response.

Neglecting the Fermi level pinning at the metal/SWCNT junction, the Schottky barrier for holes should follow the Schottky-Mott rule that can be expressed as follows Eq.(8)

$$\phi_B = \frac{E_G}{2} + \phi_{CNT} - \phi_{Pd} \quad (8)$$

Where (E_G) is the energy band gap defined by $E_G = \left(\frac{0.8301nm}{d}\right) eV$ [49], where d is the SWCNT diameter expressed in nm. A more detailed characterization of the SWCNT used for the gas-sensing devices is provided in the SI, showing that the mean diameter of the SWCNT is around 1.4 nm. Using in Eq.(8) the value of ϕ_B (plotted in **Figure 3.c**) and considering a ϕ_{CNT}= 4.9 eV [50] with a tube diameter of 1.4 nm (see **Figure 1.d**), the metal work function variation under NO_2 exposure can be estimated (see **Figure 4.b**). The metal (Pd) work function without NO_2 (concentration at 0 ppm) is found to be around 5.1 eV, which is consistent with the theoretical value [51]. After device exposure at 10 ppm of NO_2, an increment of 30 meV the Pd work function is estimated, see **Figure 4.b**. In a very interesting work driven by Dube et. al [52], similarly results are reported, where the metal work function variation as a function of the NO_2 concentration is estimated. In the mentioned study, the Pd work function variation is 4 meV, for a device based on a network SWCNT-FET, exposed to N_2 atmosphere and subsequently to 16 ppm of NO_2 molecules. The difference obtained in the two calculations can be explained by the different

approximation used in both work. In our work, for instance, the calcule is highly dependent on the measure of the flat band voltage, which is challenging to determine in the case of SWCN-FET device, while in the work of Dube et. al[52] parameter are extracted by "fitting by eyes" the experimental curve with the calculated one.

It is important to highlight that direct measurements of these values are far from straightforward[46]. Considering our proposed approach, based on indirect measurements, such a method enables an easier assessment of the Schottky barrier height, even if this value is highly dependent on the precise measurement of the flat band voltage. The obtained results show that the response variation is strongly related to the interaction of the gas molecules at the metal/SWCNT junction and these results may provide a useful basis for various nanoelectronic applications of SWCNT-FET.

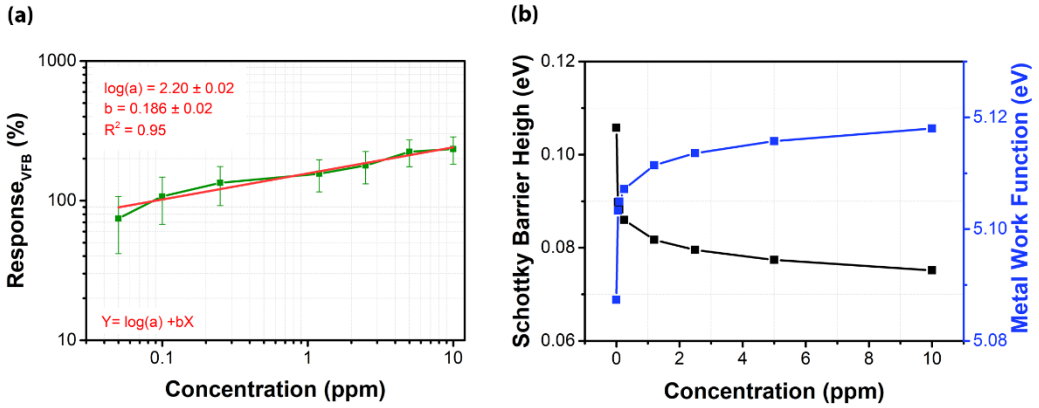

Figure 4. (a) Response calculated at the flat-band voltage. (b) Schottky barrier height and metal work function variation as function of the concentration neglecting Fermi pinning effects.

4. Conclusion

The present work sets the basis for an improved design of a next generation of gas-sensing devices based on 1D nanostructures and simultaneously provides an alternative to estimate the changes of Schottky barrier heights under the influence of gas molecules. Thanks to a smart configuration of several SWCNTs directly connected between the source and drain electrodes, the proposed devices exhibit an ultra-sensitive behavior when exposed to NO_2 molecules and are operational at room

temperature without any functionalization process. Concentrations ranging from 100 ppb up to 10 ppm were detected and the results have been shown to follow a 2 power law relation between NO_2 concentration and the response. The device response is attributed to an exponential dependence of the Schottky barrier height in the presence of NO_2 molecules. The calculation of the metal electrode work function and the Schottky barrier height at the nanotube-metal junction that explains the sensitive mechanisms has been extrapolated using an interesting approach which considers the changes of transistors transfer curves under exposure to different NO_2 concentrations. This procedure significantly simplifies the methodology for extractions of Schottky barrier values and may provide a useful basis for various nanoelectronics applications of SWCNT-FETs.

Acknowledgements

L. S. and S. F. gratefully acknowledge financial support from the Chaire de Recherche PSA AC3M sponsored by Citroën at Ecole Polytechnique and Chaire EXXI sponsored by EDF at Ecole Polytechnique. We acknowledge the Centre interdiscipinaire de microscopie électronique de l'X (CIMEX). The authors acknowledge financial support from the French state managed by the National Research Agency under the Investments for the Future program under the references ANR-10-EQPX-50 and ANR-10-EQPX-0048. This work is part of the NanoMaDe-3E Initiative

Formatting of funding sources

This work was supported by Chaire de Recherche PSA AC3M sponsored by Citroën at Ecole Polytechnique and Chaire EXXI sponsored by EDF at Ecole Polytechnique.

References

[1] J. Zhang, X. Liu, G. Neri, N. Pinna, Nanostructured Materials for Room-Temperature Gas Sensors, Adv. Mater. 28 (2016) 795–831. doi:10.1002/adma.201503825.

[2] J.S. Lee, O.S. Kwon, S.J. Park, E.Y. Park, S.A. You, H. Yoon, J. Jang, Fabrication of

ultrafine metal-oxide-decorated carbon nanofibers for DMMP sensor application, ACS Nano. 5 (2011) 7992–8001. doi:10.1021/nn202471f.

[3] J. Park, J. Kim, K. Kim, S.-Y. Kim, W.H. Cheong, K. Park, J.H. Song, G. Namgoong, J.J. Kim, J. Heo, F. Bien, J.-U. Park, Wearable, wireless gas sensors using highly stretchable and transparent structures of nanowires and graphene, Nanoscale. 8 (2016) 10591–10597. doi:10.1039/C6NR01468B.

[4] A.N. Abbas, B. Liu, L. Chen, Y. Ma, S. Cong, N. Aroonyadet, M. Köpf, T. Nilges, C. Zhou, Black phosphorus gas sensors, ACS Nano. 9 (2015) 5618–5624. doi:10.1021/acsnano.5b01961.

[5] H. Tang, Y. Li, R. Sokolovskij, L.N. Sacco, H. Zheng, H. Ye, H. Yu, X. Fan, H. Tian, T.-L. Ren, G. Zhang, Ultra-high sensitive NO2 gas sensor based on tunable polarity transport in CVD-WS2/IGZO p-N heterojunction, ACS Appl. Mater. Interfaces. (2019). doi:10.1021/acsami.9b13773.

[6] P. Bondavalli, P. Legagneux, D. Pribat, Carbon nanotubes based transistors as gas sensors: State of the art and critical review, Sensors Actuators, B Chem. 140 (2009) 304–318. doi:10.1016/j.snb.2009.04.025.

[7] Y. Zhao, J. Cai, H. Luo, S. Kang, W. Qian, C. Dong, Low pressure hydrogen sensing based on carbon nanotube field emission: Mechanism of atomic adsorption induced work function effects, Carbon N. Y. 124 (2017) 669–674. doi:10.1016/j.carbon.2017.09.032.

[8] M.M. Shulaker, G. Hills, R.S. Park, R.T. Howe, K. Saraswat, H.S.P. Wong, S. Mitra, Three-dimensional integration of nanotechnologies for computing and data storage on a single chip, Nature. 547 (2017) 74–78. doi:10.1038/nature22994.

[9] S.W. Lee, W. Lee, Y. Hong, G. Lee, D.S. Yoon, Recent advances in carbon material-based NO2gas sensors, Sensors Actuators, B Chem. 255 (2018) 1788–1804. doi:10.1016/j.snb.2017.08.203.

[10] M. Jeon, B. Choi, J. Yoon, D.M. Kim, D.H. Kim, I. Park, S.J. Choi, Enhanced sensing of

gas molecules by a 99.9% semiconducting carbon nanotube-based field-effect transistor sensor, Appl. Phys. Lett. 111 (2017) 22102. doi:10.1063/1.4991970.

[11] X. Liu, Z. Luo, S. Han, T. Tang, D. Zhang, C. Zhou, Band engineering of carbon nanotube field-effect transistors via selected area chemical gating, Appl. Phys. Lett. 86 (2005) 1–3. doi:10.1063/1.1944898.

[12] A. Boyd, I. Dube, G. Fedorov, M. Paranjape, P. Barbara, Gas sensing mechanism of carbon nanotubes: From single tubes to high-density networks, Carbon N. Y. 69 (2014) 417–423. doi:10.1016/j.carbon.2013.12.044.

[13] N. Peng, Q. Zhang, C.L. Chow, O.K. Tan, N. Marzari, Sensing mechanisms for carbon nanotube based NH3 gas detection, Nano Lett. 9 (2009) 341–357. doi:10.1021/nl803930w.

[14] V. Schroeder, S. Savagatrup, M. He, S. Lin, T.M. Swager, Carbon Nanotube Chemical Sensors, Chem. Rev. 119 (2019) 599–663. doi:10.1021/acs.chemrev.8b00340.

[15] S. Kumar, G.B. Blanchet, M.S. Hybertsen, J.Y. Murthy, M.A. Alam, Performance of carbon nanotube-dispersed thin-film transistors, Appl. Phys. Lett. 89 (2006). doi:10.1063/1.2357852.

[16] P.G. Collins, M.S. Arnold, P. Avouris, Engineering carbon nanotubes and nanotube circuits using electrical breakdown, Science (80-.). 292 (2001) 706–709. doi:10.1126/science.1058782.

[17] K. Chikkadi, M. Muoth, C. Roman, M. Haluska, C. Hierold, Advances in NO2 sensing with individual single-walled carbon nanotube transistors, Beilstein J. Nanotechnol. 5 (2014) 2179–2191. doi:10.3762/bjnano.5.227.

[18] Y. Li, M. Hodak, W. Lu, J. Bernholc, Mechanisms of NH3 and NO2 detection in carbon-nanotube-based sensors: An ab initio investigation, Carbon N. Y. 101 (2016) 177–183. doi:10.1016/j.carbon.2016.01.092.

[19] J. Suehiro, H. Imakiire, S. Hidaka, W. Ding, G. Zhou, K. Imasaka, M. Hara, Schottky-type response of carbon nanotube NO2 gas sensor fabricated onto aluminum electrodes by

dielectrophoresis, Sensors Actuators B Chem. 114 (2006) 943–949. doi:10.1016/j.snb.2005.08.043.

[20] D. Kumar, P. Chaturvedi, P. Saho, P. Jha, A. Chouksey, M. Lal, J.S.B.S. Rawat, R.P. Tandon, P.K. Chaudhury, Effect of single wall carbon nanotube networks on gas sensor response and detection limit, Sensors Actuators, B Chem. 240 (2017) 1134–1140. doi:10.1016/j.snb.2016.09.095.

[21] H.D. Jing Kong, Nathan R. Franklin, Chongwu Zhou, Michael G. Chapline, Shu Peng, Kyeongjae Cho, Nanotube Molecular Wires as Chemical Sensors, Science (80-.). 287 (2000) 622–625. doi:10.1126/science.287.5453.622.

[22] M. Lucci, A. Reale, A. Di Carlo, S. Orlanducci, E. Tamburri, M.L. Terranova, I. Davoli, C. Di Natale, A. D'Amico, R. Paolesse, Optimization of a NOx gas sensor based on single walled carbon nanotubes, Sensors Actuators B Chem. 118 (2006) 226–231. doi:10.1016/J.SNB.2006.04.027.

[23] K. Chikkadi, M. Muoth, W. Liu, V. Maiwald, C. Hierold, Enhanced signal-to-noise ratio in pristine, suspended carbon nanotube gas sensors, Sensors Actuators B Chem. 196 (2014) 682–690. doi:10.1016/J.SNB.2014.02.058.

[24] J. Li, Y. Lu, Q. Ye, M. Cinke, J. Han, M. Meyyappan, Carbon Nanotube Sensors for Gas and Organic Vapor Detection, Nano Lett. 3 (2003) 929–933. doi:10.1021/nl034220x.

[25] K. Xu, C. Wu, X. Tian, J. Liu, M. Li, Y. Zhang, Z. Dong, Single-Walled Carbon Nanotube-Based Gas Sensors for NO2 Detection, Integr. Ferroelectr. 135 (2012) 132–137. doi:10.1080/10584587.2012.685424.

[26] H. Xie, R. Zhang, Y. Zhang, Z. Yin, M. Jian, F. Wei, Preloading catalysts in the reactor for repeated growth of horizontally aligned carbon nanotube arrays, Carbon N. Y. 98 (2016) 157–161. doi:https://doi.org/10.1016/j.carbon.2015.11.001.

[27] K. Otsuka, T. Inoue, Y. Shimomura, S. Chiashi, S. Maruyama, Water-assisted self-sustained burning of metallic single-walled carbon nanotubes for scalable transistor fabrication, Nano

Res. 10 (2017) 3248–3260. doi:10.1007/s12274-017-1648-6.

[28] J. Chung, K.-H. Lee, J. Lee, R.S. Ruoff, Toward Large-Scale Integration of Carbon Nanotubes, Langmuir. 20 (2004) 3011–3017. doi:10.1021/la035726y.

[29] B.K. Sarker, N. Kang, S.I. Khondaker, High performance semiconducting enriched carbon nanotube thin film transistors using metallic carbon nanotubes as electrodes, Nanoscale. 6 (2014) 4896–4902. doi:10.1039/C3NR06470K.

[30] L. Sacco, I. Florea, M. Châtelet, C.-S. Cojocaru, Electrical and morphological behavior of carbon nanotubes synthesized within porous anodic alumina templates, J. Phys. Mater. 1 (2018) 015004. doi:10.1088/2515-7639/aad57f.

[31] A. Castan, S. Forel, L. Catala, I. Florea, F. Fossard, F. Bouanis, A. Andrieux-Ledier, S. Mazerat, T. Mallah, V. Huc, A. Loiseau, C.S. Cojocaru, New method for the growth of single-walled carbon nanotubes from bimetallic nanoalloy catalysts based on Prussian blue analog precursors, Carbon N. Y. 123 (2017) 583–592. doi:10.1016/j.carbon.2017.07.058.

[32] S. Forel, A. Castan, H. Amara, I. Florea, F. Fossard, L. Catala, C. Bichara, T. Mallah, V. Huc, A. Loiseau, C.-S. Cojocaru, Tuning bimetallic catalysts for a selective growth of SWCNTs, Nanoscale. 11 (2019) 4091–4100. doi:10.1039/C8NR09589B.

[33] A. Jorio, R. Saito, J.H. Hafner, C.M. Lieber, M. Hunter, T. McClure, G. Dresselhaus, M.S. Dresselhaus, Structural (n,m) Determination of Isolated Single-Wall Carbon Nanotubes by Resonant Raman Scattering, Phys. Rev. Lett. 86 (2001) 1118–1121. doi:10.1103/PhysRevLett.86.1118.

[34] J. Appenzeller, M. Radosavljević, J. Knoch, P. Avouris, Tunneling Versus Thermionic Emission in One-Dimensional Semiconductors, Phys. Rev. Lett. 92 (2004) 4. doi:10.1103/PhysRevLett.92.048301.

[35] P.R. Yasasvi Gangavarapu, P.C. Lokesh, K.N. Bhat, A.K. Naik, Graphene Electrodes as Barrier-Free Contacts for Carbon Nanotube Field-Effect Transistors, IEEE Trans. Electron Devices. 64 (2017) 4335–4339. doi:10.1109/TED.2017.2741061.

[36] Y.F. Chen, M.S. Fuhrer, Tuning from thermionic emission to ohmic tunnel contacts via doping in schottky-barrier nanotube transistors, Nano Lett. 6 (2006) 2158–2162. doi:10.1021/nl061379b.

[37] S. Jejurikar, D. Casterman, P.B. Pillai, O. Petrenko, M.M. De Souza, A. Tahraoui, C. Durkan, W.I. Milne, Anomalous n-type electrical behaviour of Pd-contacted CNTFET fabricated on small-diameter nanotube, Nanotechnology. 21 (2010). doi:10.1088/0957-4484/21/21/215202.

[38] A. Pacheco-Sanchez, M. Claus, Device design-enabled Schottky barrier height extraction for nanoFETs based on the 1D Landauer-Büttiker equation, Appl. Phys. Lett. 111 (2017). doi:10.1063/1.4998807.

[39] M. Freitag, J.C. Tsang, A. Bol, D. Yuan, J. Liu, P. Avouris, Imaging of the schottky barriers and charge depletion in carbon nanotube transistors, Nano Lett. 7 (2007) 2037–2042. doi:10.1021/nl070900e.

[40] X. Cui, M. Freitag, R. Martel, L. Brus, P. Avouris, Controlling energy-level alignments at carbon nanotube/Au contacts, Nano Lett. 3 (2003) 783–787. doi:10.1021/nl034193a.

[41] Q. Cao, S. Han, A. V Penumatcha, M.M. Frank, G.S. Tulevski, J. Tersoff, W.E. Haensch, Origins and Characteristics of the Threshold Voltage Variability of Quasiballistic Single-Walled Carbon Nanotube Field-E ff ect Transistors, (2015) 1936–1944.

[42] S. Heinze, J. Tersoff, P. Avouris, Electrostatic engineering of nanotube transistors for improved performance Electrostatic engineering of nanotube transistors for improved performance, 5038 (2011). doi:10.1063/1.1632531.

[43] D.J. Perello, S. ChuLim, S.J. Chae, I. Lee, M.J. Kim, Y.H. Lee, M. Yun, Anomalous Schottky Barriers and Contact Band-to-Band Tunneling in Carbon Nanotube Transistors, ACS Nano. 4 (2010) 3103–3108. doi:10.1021/nn100328a.

[44] Y. Wada, Y. Fujita, K. Takei, T. Arie, S. Akita, Suspended single-walled carbon-nanotube field-effect transistor for gas sensing application, Jpn. J. Appl. Phys. 54 (2015).

doi:10.7567/JJAP.54.06FB01.

[45] J. Zhang, A. Boyd, A. Tselev, M. Paranjape, P. Barbara, Mechanism of NO2 detection in carbon nanotube field effect transistor chemical sensors, Appl. Phys. Lett. 88 (2006) 123112. doi:10.1063/1.2187510.

[46] J. Svensson, E.E.B. Campbell, Schottky barriers in carbon nanotube-metal contacts, J. Appl. Phys. 110 (2011). doi:10.1063/1.3664139.

[47] S. Das, H.Y. Chen, A.V. Penumatcha, J. Appenzeller, High performance multilayer MoS2 transistors with scandium contacts, Nano Lett. 13 (2013) 100–105. doi:10.1021/nl303583v.

[48] J. Svensson, A.A. Sourab, Y. Tarakanov, D.S. Lee, S.J. Park, S.J. Baek, Y.W. Park, E.E.B. Campbell, The dependence of the Schottky barrier height on carbon nanotube diameter for Pd-carbon nanotube contacts, Nanotechnology. 20 (2009). doi:10.1088/0957-4484/20/17/175204.

[49] E. Joselevich, C.M. Lieber, Vectorial Growth of Metallic and Semiconducting Single-Wall Carbon Nanotubes, Nano Lett. 2 (2002) 1137–1141. doi:10.1021/nl025642u.

[50] S. Suzuki, C. Bower, Y. Watanabe, O. Zhou, Work functions and valence band states of pristine and Cs-intercalated single-walled carbon nanotube bundles, Appl. Phys. Lett. 76 (2000) 4007–4009. doi:10.1063/1.126849.

[51] H.B. Michaelson, The work function of the elements and its periodicity, J. Appl. Phys. 48 (1977) 4729–4733. doi:10.1063/1.323539.

[52] I. Dube, D. Jiménez, G. Fedorov, A. Boyd, I. Gayduchenko, M. Paranjape, P. Barbara, Understanding the electrical response and sensing mechanism of carbon-nanotube-based gas sensors, Carbon N. Y. 87 (2015) 330–337. doi:10.1016/j.carbon.2015.01.060.